

# Novel Analysis to Quantify Plume Crosswind Heterogeneity Applied to Biomass Burning Smoke

Zachary C. J. Decker, Siyuan Wang, Ilann Bourgeois, Pedro Campuzano Jost, Matthew M. Coggon, Joshua P. DiGangi, Glenn S. Diskin, Frank M. Flocke, Alessandro Franchin, Carley D. Fredrickson, Georgios I. Gkatzelis, Samuel R. Hall, Hannah Halliday, Katherine Hayden, Christopher D. Holmes, L. Gregory Huey, Jose L. Jimenez, Young Ro Lee, Jakob Lindaas, Ann M. Middlebrook, Denise D. Montzka, J. Andrew Neuman, John B. Nowak, Demetrios Pagonis, Brett B. Palm, Jeff Peischl, Felix Piel, Pamela S. Rickly, Michael A. Robinson, Andrew W. Rollins, Thomas B. Ryerson, Kanako Sekimoto, Joel A. Thornton, Geoff S. Tyndall, Kirk Ullmann, Patrick R. Veres, Carsten Warneke, Rebecca A. Washenfelder, Andrew J. Weinheimer, Armin Wisthaler, Caroline Womack, and Steven S. Brown\*



Cite This: *Environ. Sci. Technol.* 2021, 55, 15646–15657



Read Online

ACCESS |

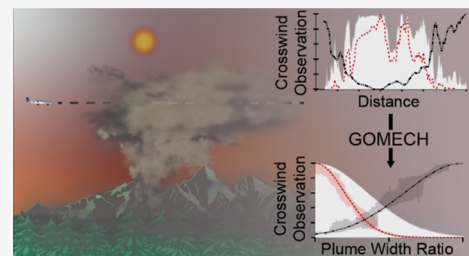
Metrics & More

Article Recommendations

Supporting Information

**ABSTRACT:** We present a novel method, the Gaussian observational model for edge to center heterogeneity (GOMECH), to quantify the horizontal chemical structure of plumes. GOMECH fits observations of short-lived emissions or products against a long-lived tracer (e.g., CO) to provide relative metrics for the plume width ( $w_i/w_{\text{CO}}$ ) and center ( $b_i/w_{\text{CO}}$ ). To validate GOMECH, we investigate OH and  $\text{NO}_3$  oxidation processes in smoke plumes sampled during FIREX-AQ (Fire Influence on Regional to Global Environments and Air Quality, a 2019 wildfire smoke study). An analysis of 430 crosswind transects demonstrates that nitrous acid (HONO), a primary source of OH, is narrower than CO ( $w_{\text{HONO}}/w_{\text{CO}} = 0.73–0.84 \pm 0.01$ ) and maleic anhydride (an OH oxidation product) is enhanced on plume edges ( $w_{\text{maleicanhydride}}/w_{\text{CO}} = 1.06–1.12 \pm 0.01$ ). By contrast,  $\text{NO}_3$  production [ $\text{P}(\text{NO}_3)$ ] occurs mainly at the plume center ( $w_{\text{P}(\text{NO}_3)}/w_{\text{CO}} = 0.91–1.00 \pm 0.01$ ). Phenolic emissions, highly reactive to OH and  $\text{NO}_3$ , are narrower than CO ( $w_{\text{phenol}}/w_{\text{CO}} = 0.96 \pm 0.03$ ,  $w_{\text{catechol}}/w_{\text{CO}} = 0.91 \pm 0.01$ , and  $w_{\text{methylcatechol}}/w_{\text{CO}} = 0.84 \pm 0.01$ ), suggesting that plume edge phenolic losses are the greatest. Yet, nitrophenolic aerosol, their oxidation product, is the greatest at the plume center ( $w_{\text{nitrophenolic aerosol}}/w_{\text{CO}} = 0.95 \pm 0.02$ ). In a large plume case study, GOMECH suggests that nitrocatechol aerosol is most associated with  $\text{P}(\text{NO}_3)$ . Last, we corroborate GOMECH with a large eddy simulation model which suggests most (55%) of nitrocatechol is produced through  $\text{NO}_3$  in our case study.

**KEYWORDS:** phenolics, catechol, HONO, LES model, plume shape, wildfire, biomass burning, FIREX-AQ



## INTRODUCTION

Biomass burning (BB), including wildfires, has an increasing impact on air quality at local, regional, and global scales.<sup>1</sup> BB emits  $\text{NO}_x$  ( $\text{NO} + \text{NO}_2$ ), nitrous acid (HONO), volatile organic compounds (BVOCs), and particulate matter that evolve chemically with age.<sup>2–8</sup> Similar to plumes from urban and electric power generation sources,<sup>9–11</sup> BB plume chemistry varies in the crosswind dimension during plume advection.<sup>12</sup> BB plumes are unique because they contain large amounts of primary and secondary aerosols, which amplify the chemical differences between the plume center and edge through plume darkening, or the attenuation of sunlight, concentrated at the plume center.<sup>12,13</sup>

Differences in sunlight between the center and edge of BB plumes may result in differences in the amount and reactivity

of atmospheric oxidants such as the hydroxyl radical (OH), ozone ( $\text{O}_3$ ), and the nitrate radical ( $\text{NO}_3$ ). For example, Peng et al. showed that in wildfire plumes, the photolysis of HONO (R1) can be the dominant source of OH and that it occurs at greater rates on plume edges relative to the center.<sup>12</sup>



Received: June 10, 2021

Revised: November 9, 2021

Accepted: November 10, 2021

Published: November 24, 2021



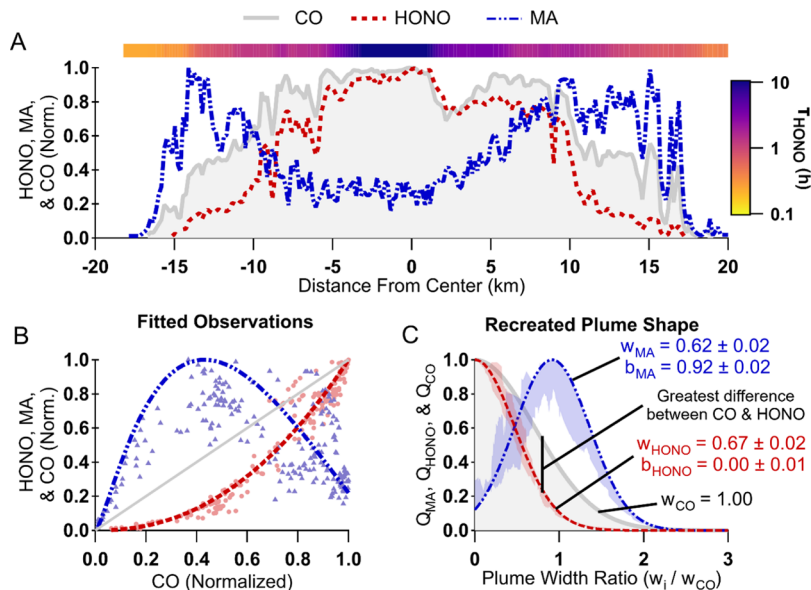


**Figure 1.** Panel (A): Normalized observations of HONO (red), MA (measured as  $\text{C}_4\text{H}_2\text{O}_3$ ) (blue), and CO (gray outline and fill) as well as HONO photolytic lifetime in hours ( $\tau_{\text{HONO}}$ , color scale) plotted against distance from the plume center (maximum CO) from a plume transect of the WF fire sampled by the DC-8 at 01:22 UTC on Aug 8 2019. Average plume age was 1.2 h but varied between 1 and 1.25 h within the transect. Panel (B): Normalized observations of HONO (red circles), MA (blue triangles), and CO (gray line) plotted against normalized CO with fits (using eq 2) of MA (blue) and HONO (red). Panel (C): Recreated plume shapes of HONO (red) and MA (blue) using the fit parameters derived in panel (B) as well as shading indicating fit residuals averaged by normalized CO bins of 0.004. The recreated plume shapes suggest that HONO is  $33 \pm 2\%$  narrower than CO and MA is  $38 \pm 2\%$  narrower than CO, but the maximum MA is shifted to a CO plume width of  $0.92 \pm 0.02$ .

Further, OH concentrations are expected to depend nonlinearly on  $\text{NO}_x$ , which can vary in concentration in the crosswind dimension.<sup>14</sup>

Entrainment of background  $\text{O}_3$ , as well as photochemical production, can provide  $\text{O}_3$  for plume oxidation near the plume edges.<sup>15</sup> Further, NO can depress  $\text{O}_3$  at the plume center in freshly emitted plumes.

The role of  $\text{NO}_3$  in daytime BB plumes has generally been neglected or expected to occur primarily at the plume center where photolysis rates are depressed.<sup>7,8,16,17</sup> The  $\text{NO}_3$  radical is formed by the gas-phase reaction of  $\text{O}_3$  and  $\text{NO}_2$  (R2).



In urban plumes during the daytime, the  $\text{NO}_3$  radical is rapidly destroyed by photolysis and by reaction with NO ( $\tau < 10$  s).<sup>18,19</sup> The nitrate radical is also a precursor for  $\text{N}_2\text{O}_5$ , which undergoes heterogeneous uptake to produce  $\text{ClNO}_2$  and  $\text{HNO}_3$ .<sup>19–21</sup>

Despite these potential loss pathways, plume center models suggest that most of the  $\text{NO}_3$  is expected to be lost to BVOCs.<sup>8,13</sup>

This is due, in part, to phenolics that react with  $\text{NO}_3$  near the gas-kinetic limit to form nitrophenolics and secondary organic aerosol (SOA).<sup>7,8,22–25</sup> Nitrophenolics absorb strongly in the ultraviolet and visible regions of the solar spectrum and are expected to significantly contribute to brown carbon (BrC) absorption.<sup>7,16,26</sup> Phenolic reactions with OH in the presence of  $\text{NO}_x$  also form nitrophenolics but at a lower yield.<sup>22</sup>

Plume sampling by research aircraft is often conducted perpendicular to the direction of transport, the crosswind dimension, which reveals complex structures that reflect the heterogeneity in emission and chemistry.<sup>7,27</sup> While plume structures vary in the crosswind vertical dimension as well, we focus only on the horizontal dimension in this work. Analysis of chemical evolution in plumes often avoids an analysis of

plume heterogeneity and mixing by integrating the observations across the plume horizontally or by only considering plume center observations.<sup>8,12,13,28–32</sup> Plume dispersion models represent one approach to quantify the spatial variation of plumes.<sup>33</sup> Another includes high-resolution Eulerian models<sup>15,34,35</sup> or turbulence-resolving models (large eddy simulation, LES);<sup>36</sup> however, these are computationally expensive and therefore include limited chemistry. When the crosswind plume structure is considered, it is often studied as a function of distance from the plume center (e.g., Figure 1A), which makes the task of comparing plume heterogeneity as a function of age difficult because plumes tend to grow in size with age downwind of the source.

We describe a novel method, the Gaussian observational model for edge to center heterogeneity (GOMECH), that quantitatively describes plume structures in the crosswind horizontal relative to a long-lived tracer. GOMECH is capable of separating differential crosswind plume production and loss rates between a short-lived compound of interest and a long-lived tracer. We present GOMECH and use it to investigate several major chemical processes related to OH and  $\text{NO}_3$  oxidation, with an emphasis on phenolic compounds, in fire plumes observed by both the NOAA Twin Otter and NASA DC-8 aircraft during the Fire Influence on Regional to Global Environments and Air Quality (FIREX-AQ) study, described below. First, we use GOMECH to model the plume structure of OH and  $\text{NO}_3$  using the chemical proxies HONO, MA, peroxy acetyl nitrate (PAN),  $\text{O}_3$ , and  $\text{NO}_3$  production rate as well as phenolics and nitrophenolics in a bulk analysis of 430 crosswind transects. Finally, we consider a case study of a large wildfire to elucidate the relationships of OH,  $\text{NO}_3$ , and aerosol nitrocatechol (NC) plume structures by GOMECH and an LES model.

## METHODS

**Aircraft Measurements.** Both the NOAA Twin Otter and the NASA DC-8 aircraft sampled wildfire smoke as part of FIREX-AQ during the summer of 2019 in the United States. Below, we briefly describe the instrumentation used for this analysis, which are described further, along with plume age estimation<sup>37</sup> in the *Supporting Information* and Table S1.

From the Twin Otter, this analysis uses observations of BBVOCs and HONO from a iodide high-resolution time-of-flight chemical ionization mass spectrometer<sup>38</sup> ( $\text{I}^-$  HR-ToF-CIMS, 2 Hz). A commercial cavity ringdown spectrometer (Picarro G2401-m) provided measurements of CO<sup>39</sup> (0.5 Hz), and a custom chemiluminescence instrument<sup>40</sup> measured NO,  $\text{NO}_2$ , and  $\text{O}_3$  (1 Hz). Measurements of a group of particle-phase nitrophenolic ions (Table S1)<sup>7</sup> are from an HR-ToF aerosol mass spectrometer (HR-ToF AMS, 1 Hz).<sup>7,41,42</sup>

From the DC-8, we use measurements of CO from a tunable diode laser spectrometer<sup>43</sup> (1 Hz) when available and from a cavity enhanced spectrometer<sup>44</sup> (CES, 1 Hz) when the diode laser spectrometer data were unavailable. Measurements of  $\text{CH}_4$  are also from the tunable diode laser spectrometer<sup>43</sup> (1 Hz). Measurements of  $\text{NO}_2$  and  $\text{O}_3$  are provided by a chemiluminescence<sup>45–47</sup> (CL, 1 Hz) instrument. When measurements of  $\text{NO}_2$  by the CL instrument are unavailable, we use measurements by a CES<sup>48</sup> (1 Hz). We use measurements of NO by a laser-induced fluorescence instrument<sup>49</sup> (1 Hz). Measurements of  $\text{C}_4\text{H}_2\text{O}_3$  (likely maleic anhydride, MA) were taken from three instruments: (1) a proton transfer reaction ToF-MS<sup>50</sup> (PTR-ToF-MS, 1 Hz) for all flights except 7 Aug 2019 when the instrument was not operational, (2) a second PTR-ToF-MS<sup>51–53</sup> on 7 Aug, and (3) from an  $\text{I}^-$  ToF-CIMS<sup>32,54</sup> on 7 Aug. Measurements of HONO are also taken from the  $\text{I}^-$  ToF-CIMS<sup>32,54</sup> (1 Hz). PAN measurements were performed by a thermal dissociation CIMS<sup>55</sup> (1 Hz). Measurements of aerosol NC measured as  $\text{C}_6\text{H}_5\text{NO}_4$  were taken from an extractive electrospray ionization ToF-MS<sup>56</sup> (EESI-MS, 1 Hz). Aerosol NC from the EESI-MS correlates well ( $R^2 = 0.75$ , Figure S1) with two nitrophenolic ions from an HR-ToF AMS<sup>57,58</sup> aboard the DC-8, which are also used from the HR-ToF AMS aboard the Twin Otter. Photolysis rates of HONO (jHONO) were determined from spectrally resolved measurements from the charged-coupled device actinic flux spectroradiometers (1 Hz).<sup>59</sup>

**LES Model.** We analyze model results from a LES of the Williams Flats (WF) fire that was previously described by Wang et al.<sup>36,60,61</sup> with the addition of catechol oxidation mechanisms for  $\text{NO}_3$ , OH, and  $\text{O}_3$  (see *Supporting Information* Section 2 and Table S2). Our mechanism includes gas-phase formation of NC only, which is assumed to partition entirely to the particle phase.

**Derivation of the GOMECH.** Section 3 of the *Supporting Information* provides a detailed derivation of GOMECH, which is briefly outlined below. Dispersion of a point source emission leads to a Gaussian shape as a function of crosswind distance ( $y$ ) that is symmetric about the plume center ( $y = 0$ ).<sup>62</sup> We define the plume center as the location of the maximum observed CO, a long-lived BB emission. The crosswind structure of CO is thus

$$\text{CO} = A_{\text{CO}} e^{-y^2/w_{\text{CO}}^2} \quad (1)$$

Here,  $A_{\text{CO}}$  is the maximum of CO and  $w_{\text{CO}}$  is the plume width of CO. The plume width is defined as the distance from the plume center to the location where  $\text{CO} = A_{\text{CO}} e^{-1}$  or  $w_{\text{CO}} = y$ .

Similarly, for a species  $i$ , the crosswind structure is

$$i = A_i e^{-(y-b)^2/w_i^2} \quad (2)$$

where  $A_i$  is the maximum of  $i$ ,  $w_i$  is the plume width of  $i$ , and  $b$  is the location of maximum  $i$  relative to the plume center of CO. The variable  $b$  accounts for measurements where the maximum of  $i$  is shifted relative to CO (e.g., MA in Figure 1A).

However, fires typically consist of a series of hot spots or a fire front that creates complex crosswind plume structures that often do not appear Gaussian when considered as a function of distance from the plume center. Under the assumption that all emissions sampled in the crosswind (1) were affected by mixing equally, (2) were colocated, and (3) did not vary with fire conditions, any change in the crosswind structure of  $i$ , relative to CO, will be due to chemistry or photolysis. To resolve the plume structure effects from chemistry or photolysis, we rederive  $i$  as a function of CO by eliminating  $y$  in both eqs 1 and 2 (see Section 3 in the *Supporting Information*) shown below, which is the full form of GOMECH.

$$i = A_i \times A_{\text{CO}}^{-w_{\text{CO}}^2/w_i^2} \times \text{CO}^{w_{\text{CO}}^2/w_i^2} \exp \left[ \frac{2b[\sqrt{w_{\text{CO}}^2 \ln(Q_{\text{CO}})} - w_{\text{CO}}^2 \ln(A_{\text{CO}})]}{w_i^2} - \frac{b^2}{w_i^2} \right] \quad (3)$$

Here, both  $b$  and  $w_i$  are relative to  $w_{\text{CO}}$ . To simplify eq 1, we define  $w_{\text{CO}}$  as 1 and normalize  $i$  and CO to a maximum of 1, which are denoted as the unitless  $Q_i$  and  $Q_{\text{CO}}$ , respectively. For measurements that are enhanced in the crosswind transect (e.g., HONO in Figure 1A), we define the ambient background signal (a 10 s average before and after the plume) as 0. For measurements depleted in the crosswind transect (e.g., MA in Figure 1A), we define 0 as the minimum observed signal in the plume. After doing so,  $Q_i$  is

$$Q_i = Q_{\text{CO}}^{1/w_i^2} \exp \left[ \frac{2b[\sqrt{\ln(Q_{\text{CO}})}]}{w_i^2} - \frac{b^2}{w_i^2} \right] \quad (4)$$

We use eq 2 to perform a least-squares fit of  $Q_i$  as a function of  $Q_{\text{CO}}$  to determine both  $w_i$  and  $b$  relative to  $w_{\text{CO}}$  for observed crosswind transects. While our analysis uses normalized observations, non-normalized observations can be used with eq 1 to find equivalent, yet unitless,  $w_i$  and  $b$  relative to  $w_{\text{CO}}$ . For further discussion on units, refer to Section 3 of the *Supporting Information*.

The concepts surrounding GOMECH are detailed with examples (Figures S2–S6) in Section 4 of the *Supporting Information*. Briefly, differences in plume structures of  $Q_i$  relative to  $Q_{\text{CO}}$  include (1) enhanced loss of  $Q_i$  on plume edges relative to the plume center or enhanced formation of  $Q_i$  at the plume center relative to the plume edge (termed narrowing, see HONO in Figure 1A) or (2) enhanced formation of  $Q_i$  at plume edges relative to the plume center or enhanced loss of  $Q_i$  at the plume center relative to the plume edge (termed widening), where either may lead to a plume edge  $Q_i$  greater than plume center ( $b > 0$ , see MA in Figure 1A).

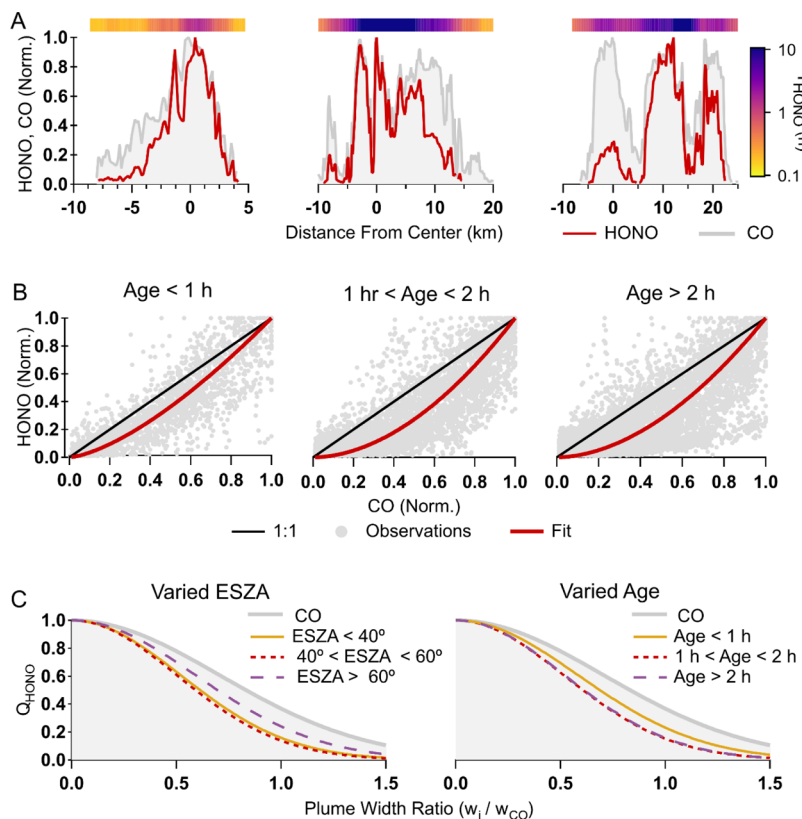


**Figure 2.** All data shown are from the DC-8 dataset. Panel (A) Examples of normalized observations of HONO (red), CO (gray fill), and HONO photolytic lifetime (color scale) plotted against distance from the plume center from three separate crosswind transects. Panel (B): Bulk analysis examples of normalized crosswind transects of HONO (gray markers) and CO (black) plotted against normalized CO with fits shown in red. Panel (C): Recreated plume shapes of HONO binned by ESZAs and plume ages, which show that the HONO plume shape is consistently narrower than CO.

The relationships above are empirical, but as described below, they fit the differential gradients of an array of short-lived species relative to CO. The text and *Supporting Information* provide uncertainty metrics to quantify the validity of this empirical approach, which is further discussed in Section 5 of the *Supporting Information*. Briefly, reported errors for  $w$  and  $b$  are the estimated standard deviation of the fit and may not capture differences in GOMECH results when using tracers other than CO, as discussed in the *Supporting Information*. Shading on GOMECH plume shapes are residuals of the fitted observations averaged per normalized CO bins of 0.004. GOMECH cannot accurately approximate the plume center of measurements that exhibit strong plume asymmetry (Figure S7). Inlet effects (such as hysteresis) can bias plume shapes (Figure S8). Last, low signal to noise can result in plume widths that are likely lower limits (for narrow plumes) or upper limits (for wide plumes). Therefore, in bulk analyses (discussed below), we exclude plumes based on signal thresholds (Table S3).

## RESULTS AND DISCUSSION

### Quantification of Photochemical Plume Structure.

Nitrous acid, HONO, is a major BB emission that undergoes rapid photolysis to produce OH radicals (R1). The HONO photolytic lifetime (i.e.,  $j_{\text{HONO}}^{-1}$ ) on the edge of a plume is of the order of tens of minutes (Figure 1A), typically more rapid than mixing time scales that reduce its differential gradient relative to CO. As such, HONO is depleted relative to CO on plume edges creating a narrow HONO plume structure,

consistent with results by Peng et al.<sup>12</sup> GOMECH analysis provides a quantitative measure of these gradients and their implications for plume photochemistry. The GOMECH fit in Figure 1B,C shows quantitatively that HONO is  $33 \pm 2\%$  narrower than CO ( $w_{\text{HONO}}/w_{\text{CO}} = 0.67 \pm 0.02$ ). Therefore, we expect that OH has been produced on the plume edges.

Indeed, we see plume edge enhancements of OH oxidation products, namely, MA (Figure 1A) and PAN (Figure S2A), on plume edges. MA is an oxidation product that results from OH oxidation of furans (see Section 6 in the *Supporting Information*).<sup>50,63–67</sup> While we find similarity in the plume structure between PAN and MA, we primarily use MA as an indicator for OH chemistry.<sup>68</sup>

GOMECH demonstrates that MA is  $38 \pm 2\%$  narrower than CO ( $w_{\text{MA}}/w_{\text{CO}} = 0.62 \pm 0.02$ ), and the maximum of MA is shifted from a CO maximum of  $w_{\text{MA}}/w_{\text{CO}} = 0.92 \pm 0.02$ . The greatest depletion of HONO relative to CO is located at  $\sim 0.81 w_{\text{CO}}$  (Figure 1C). This is near the greatest enhancement of MA, consistent with a chemical regime in which loss of HONO and production of MA are spatially similar. Additional examples are shown for HONO, PAN, O<sub>3</sub>, and  $j_{\text{HONO}}$  in Figures S2–S4.

As we demonstrate further below and in detail in the *Supporting Information*, GOMECH provides a measure of the plume structure that is qualitatively consistent with the expected chemistry, trends in plume age, and trends in photolysis history. Further, the model produces consistent results for individual compounds regardless of the research platform and measurement technique.

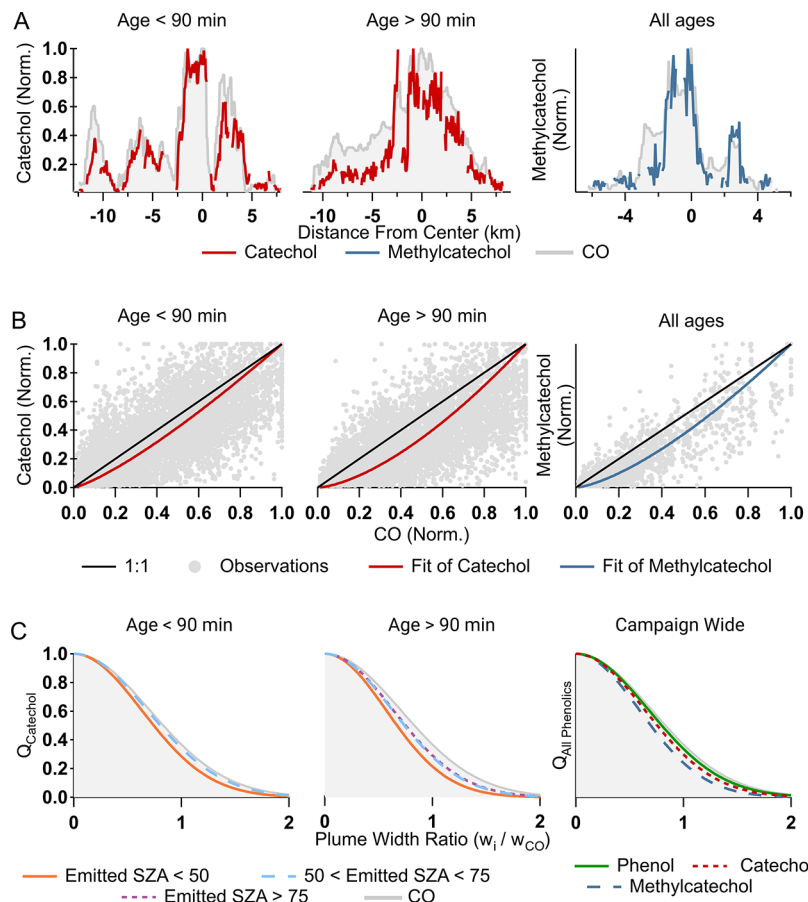


**Figure 3.** Panel (A) Examples of normalized observations of catechol (measured as  $C_6H_6O_2$ , red) and methylcatechol (measured as  $C_7H_8O_2$ , blue), and CO (gray fill) plotted against distance from the plume center from wildfire plume transects sampled by the NOAA Twin Otter. Panel (B): Bulk analysis examples of normalized crosswind transects of catechol, methylcatechol (gray markers), and CO (black) plotted against normalized CO with fits (using eq 2) shown by solid colored lines. Panel (C): Recreated plume shapes of phenol (measured as  $C_6H_6O$ , green), catechol (red dash) and methylcatechol (blue dash), as well as of catechol colored by ESZA and separated by age. Data gaps in panel (A) are from instrument zeros.

**Bulk Analysis of Photochemical Plume Structures.** Conclusions from Figure 1 apply to the majority of the observations. A bulk analysis of HONO, performed by running a single GOMECH fit on combined 210 crosswind transects from the DC-8 and a single GOMECH fit on combined 220 crosswind transects from the NOAA Twin Otter, finds average plume widths that are  $24 \pm 1\%$  ( $w_{HONO}/w_{CO} = 0.76 \pm 0.01$ ) and  $20 \pm 1\%$  ( $w_{HONO}/w_{CO} = 0.80 \pm 0.01$ ) narrower than CO, respectively. Average plume ages with  $\pm 1\sigma$  variabilities were  $2.2 \pm 1.1$  and  $2.3 \pm 1.3$  h, respectively. Thus, HONO plume structures were consistently narrower than CO across research platform and plume. Indeed, as shown by the example crosswind transects in Figure 2A, HONO plume structures appear complex but generally depleted on plume edges.

Despite this complexity, GOMECH is able to identify trends in the HONO plume width as a function of the smoke age and the solar zenith angle at the time of emission or emitted solar zenith angle (ESZA, where  $0^\circ$  is solar noon and  $90^\circ$  is sunset). ESZA is relative and qualitative measure of the rates of photolysis and provides insight into the photolysis history of sampled smoke.

HONO plumes narrow with increasing age (Figure 2B,C and Table S4). Specifically, for smoke age  $< 1$  h,  $w_{HONO}/w_{CO} = 0.83 \pm 0.01$ , and for smoke age  $> 1$  h,  $w_{HONO}/w_{CO} = 0.73 \pm 0.01$ , consistent with previous results.<sup>12</sup> Similarly, the HONO plume width is narrower for smoke emitted earlier in the day.

Specifically, for smoke emitted before late afternoon (ESZA  $< 60^\circ$ ),  $w_{HONO}/w_{CO} = 0.71 \pm 0.01$ , and for smoke emitted in the evening or later (ESZA  $> 60^\circ$ ),  $w_{HONO}/w_{CO} = 0.84 \pm 0.01$ . These results are explained by decreasing  $j_{HONO}$  with increasing ESZA. Median  $j_{HONO}^{-1}$  values were 0.45 h before late afternoon and 2.34 h in the evening or later. Replacing CO with methane, benzene, or toluene as a long-lived tracer produces similar trends (Figure S9); however, note that the width varies depending on the choice of the tracer as discussed in the Supporting Information. The  $w_{HONO}$  dependence on ESZA further reveals that HONO photolysis, and thus OH production, is larger earlier in the day.

Indeed, the MA plume width relative to CO ( $w_{MA}/w_{CO}$ ) is consistently  $> 1$  (Figure S10 and Table S5). The plume center of MA generally aligns with CO ( $b_{MA}/w_{CO} = 0$ ), unlike the example in Figure 1 (Figure S11 discussed in the Supporting Information and in a following section).  $w_{MA}/w_{CO}$  varies between  $1.06 \pm 0.01$  and  $1.12 \pm 0.04$  across plume age and ESZA. There is not a clear trend in  $w_{MA}$  with ESZA, but  $w_{MA}$  appears to decrease with age. The consistently wider plume structure of MA is indicative of enhanced OH oxidation of furans on the plume edges.

**Bulk Analysis of  $NO_3$  Plume Structure.** To investigate  $NO_3$  chemistry, we perform a GOMECH bulk analysis on the instantaneous  $NO_3$  production rate,  $P(NO_3)$ , as a measure of the potential for  $NO_3$  chemistry.<sup>19</sup>

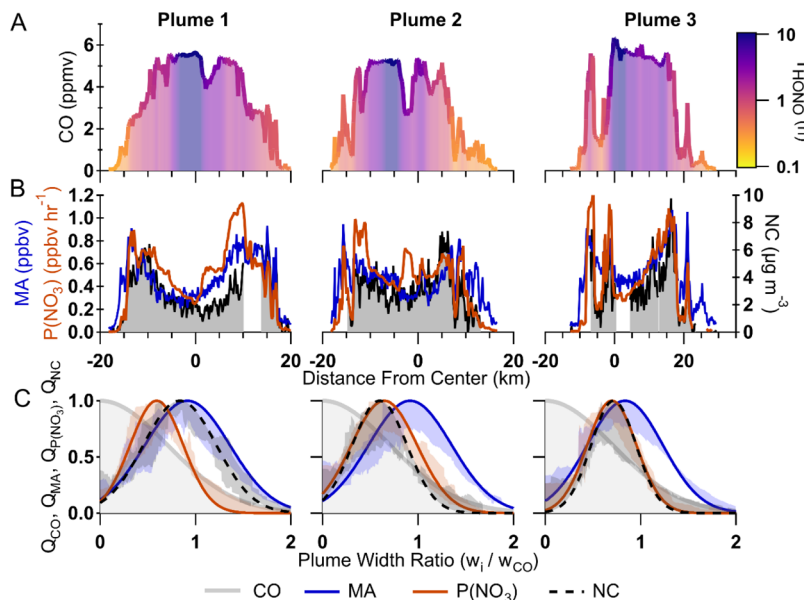


**Figure 4.** Panel (A): Observations of CO colored by HONO photolytic lifetime plotted against distance from the plume center from plume transects of the WF fire sampled by the NASA DC-8. Panel (B): Observations of MA (measured as  $C_4H_2O_3$ , blue) and aerosol NC (measured as  $C_6H_5NO_4$ , black outline and fill) as well as calculated  $P(NO_3)$  (red). Panel (C): Recreated plume shapes of MA (blue), NC (black), and  $P(NO_3)$  (red) from fit parameters shown in Figure S15 as well as shading indicating fit residuals averaged by normalized CO bins of 0.004. Data gaps for NC are due to instrument zeros. Plume ages for plumes 1, 2, and 3 are 1–1.25, 1.25–1.50, and 1.65–1.95 h.

$$P(NO_3) = k_{NO_3}[NO_2][O_3] \quad (5)$$

There is a clear trend in  $P(NO_3)$  plume width ( $w_{P(NO_3)}$ ) as a function of ESZA that is consistent across research aircraft (Figure S12 and Table S6), and plume centers are almost always aligned with CO (Figure S13 discussed in the Supporting Information and in a following section). For smoke emitted in the afternoon (ESZA < 40° from the DC-8 and ESZA < 50° on the Twin Otter; data bins differ due to differences in targeted smoke emission times by each aircraft),  $w_{P(NO_3)}/w_{CO} = 0.92 \pm 0.01$  and  $0.91 \pm 0.01$ , respectively. Smoke emitted in the evening or later (ESZA > 60° from the DC-8 and ESZA > 75° on the Twin Otter) generally aligned with CO ( $w_{P(NO_3)}/w_{CO} = 1.00 \pm 0.02$  and  $1.00 \pm 0.02$ , respectively). This suggests that the greatest enhancements of  $NO_3$  are likely at the plume center earlier in the day. Even so, the majority of plume width (91–100%), and thus emissions, will be in a region where  $P(NO_3) >$  background levels.

#### Bulk Analysis of the Phenolic Plume Structure.

Phenolic compounds are uniquely enhanced in BB emissions and are short-lived, exhibiting high reactivity to both OH and  $NO_3$ .<sup>8,22,69</sup> We investigate three masses which can be attributed to phenolics reported by the  $I^-$  CIMS aboard the Twin Otter:  $C_6H_6O$  (likely phenol),  $C_6H_6O_2$  (likely catechol), and  $C_7H_8O_2$  (likely methylcatechol).<sup>7</sup> In a bulk GOMECH analysis, the average plume widths of phenol ( $w_{phenol}/w_{CO} = 0.96 \pm 0.03$ ), catechol ( $w_{catechol}/w_{CO} = 0.91 \pm 0.01$ ), and methylcatechol ( $w_{methylcatechol}/w_{CO} = 0.84 \pm 0.01$ ) are narrower than that of CO (Figure 3 and Table S7). These widths decrease with increasing bimolecular rate coefficient<sup>69</sup> between the phenolic and  $NO_3$  or OH. As we have shown above, OH is expected to be enhanced at plume edges. Further, while  $P(NO_3)$  is expected to be enhanced at the plume center, some  $P(NO_3)$  is expected at plume edges as well. Therefore, it is likely that the narrow phenolics plume structure is caused by enhanced oxidation by both  $NO_3$  and OH on the plume edges.

Further, GOMECH shows that the catechol plume is narrower for aged smoke and for smoke emitted earlier in the day (Figure 3B,C and Table S7). For example, in aged smoke (>1.5 h) emitted early in the day (ESZA < 50°), catechol is  $19 \pm 1\%$  narrower than CO. In contrast, catechol in young smoke (age < 1.5 h) emitted later in the day (ESZA between 50–75°) is only  $3 \pm 1\%$  narrower than CO. As shown above, GOMECH suggests that OH production is enhanced on plume edges earlier in the day, while  $P(NO_3)$  is enhanced at the plume center earlier in the day. Therefore, it is likely that the apparent narrowing trend with ESZA is due to OH oxidation of catechol.

Both  $NO_3$  and OH oxidation of phenolics results in the formation of nitrophenolic SOA. Running a GOMECH bulk analysis of Twin Otter AMS nitrophenolic signals<sup>7</sup> suggests that the average nitrophenolic aerosol is  $5 \pm 2\%$  narrower than CO (Figure S14 and Table S8). A narrow plume may be the result of nitrophenolic photolysis, as suggested by Sangwan and Zhu,<sup>70,71</sup> on plume edges. However, enhanced formation at the plume center would be consistent with the enhanced plume center  $P(NO_3)$ , which is known to form nitrophenolics at a greater yield than OH<sup>22</sup> and was shown to produce the majority of nitrophenolics at the center of daytime BB plumes sampled during FIREX-AQ.<sup>13</sup>

**WF Fire Case Study.** The WF fire produced the largest plume sampled during FIREX-AQ (Figure S15). We consider four sampling patterns of the WF fire: two on 3 Aug and two on 7 Aug (Figure S16). These plumes are chosen because they had significant plume darkening at their center (90–99% attenuation of  $j_{HONO}$ ), which results in clear center-edge effects that help to differentiate the influence of OH and  $NO_3$  chemistry on the formation of nitrophenolics.

Figure 4 shows that MA, aerosol  $C_6H_5NO_4$  (attributed to NC<sup>56</sup>), and calculated  $P(NO_3)$  are depressed at the plume center and have maxima near the plume edge for the 7 Aug plume. This is the result of significantly reduced actinic flux at

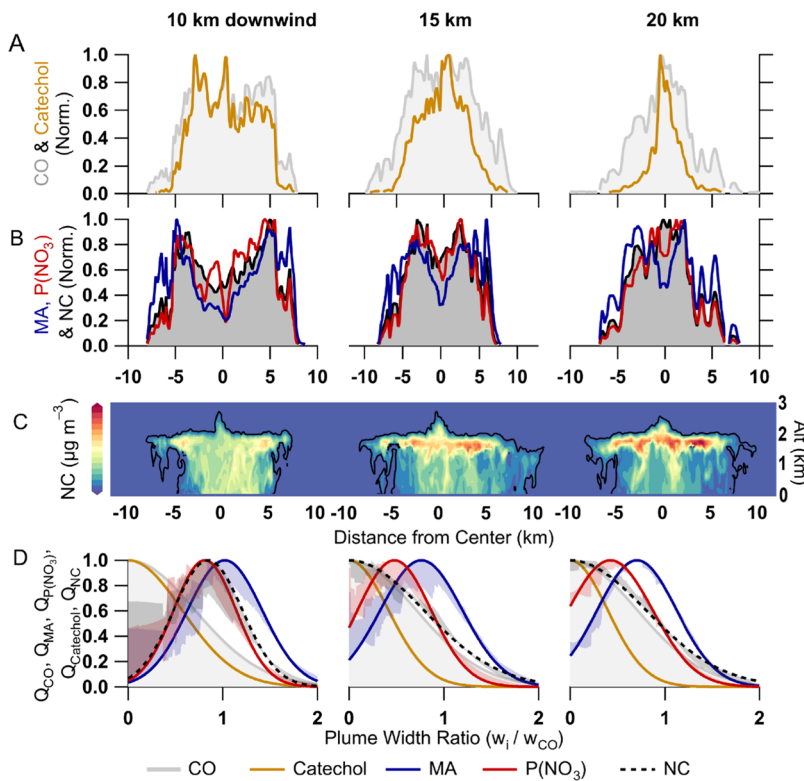


**Figure 5.** Panel (A): LES model results of CO (gray) and catechol (brown) for three crosswind transects 10, 15, and 20 km downwind of the WF fire sampled on 3 Aug 2019 by the NASA DC-8. Panel (B): LES model results for MA (blue), P(NO<sub>3</sub>) (red), and aerosol NC (black). Panel (C): LES model curtains of aerosol NC (color scale). Panel (D): GOMECH plume shapes of MA (blue), NC (black), and P(NO<sub>3</sub>) (red) from fit parameters shown in Table S10 as well as shading indicating fit residuals averaged by normalized CO bins of 0.004.

the plume center reducing photolytic OH production as well as emissions of NO titrating O<sub>3</sub> and thus P(NO<sub>3</sub>). We apply GOMECH to these observations as seen in Figure 4B–C (fits shown in Figure S17 and Table S9). We show only three young plume transects (age: 1–2 h) because GOMECH was unable to reliably locate the plume center of MA in smoke 2–3 h old likely due to issues with plume asymmetry (e.g., Figure S7).

GOMECH reveals that the plume center of NC aerosol is most similar to MA ( $\Delta b = 0.08 \pm 0.03$  and  $\Delta w = 0.09 \pm 0.03$ ) as opposed to P(NO<sub>3</sub>) ( $\Delta b = 0.25 \pm 0.02$  and  $\Delta w = 0.15 \pm 0.02$ ) in the youngest transect (left in Figure 4C). The NC aerosol shifts toward the CO plume center and becomes narrower with age until it is closely aligned with P(NO<sub>3</sub>) in the second ( $\Delta b = 0.05 \pm 0.02$  and  $\Delta w = 0.08 \pm 0.02$ ) and third ( $\Delta b = 0.02 \pm 0.01$  and  $\Delta w = 0.04 \pm 0.01$ ) transects. Our LES model suggests similar results.

We apply our LES model to the 3 Aug second pass sampling of the WF fire where we find agreement between model results and observations of NC aerosol (Figure S18). We are unable to run the LES model on the 7 Aug sampling due to complex plume dynamics.

Even so, LES model results show plume structures similar to those observed in Figure 4. Modeled NC aerosol, MA, and P(NO<sub>3</sub>) are enhanced on plume edges, while modeled catechol narrows downwind of the fire (Figure 5A–C). Further, the LES model result shows that NC formation is controlled by NO<sub>3</sub> chemistry on the plume edges, similar to GOMECH results in Figure 4D.

Applying GOMECH to crosswind transects of the LES model (Figure 5D) shows that the catechol plume width

narrows between 10 and 20 km downwind of the fire ( $w_{catechol}/w_{CO} = 0.81 \pm 0.01$  and  $w_{catechol}/w_{CO} = 0.56 \pm 0.02$ , respectively). The LES model reveals that catechol loss on plume edges is mostly due to OH oxidation. Enhanced OH oxidation on the plume edge is consistent with the plume edge enhancements of MA shown by GOMECH in Figure 5D.

While most of the catechol loss is due to OH, the cumulative production of NC aerosol is mostly (55%) from NO<sub>3</sub> chemistry (Figure S19). This is consistent with a plume center model of the WF plumes and is due to differences in NC yield from NO<sub>3</sub> and OH oxidation pathways.<sup>13</sup> Indeed, the GOMECH structure of P(NO<sub>3</sub>) and aerosol NC are closely aligned ( $\Delta b = 0.03 \pm 0.01$  and  $\Delta w = 0.04 \pm 0.03$ ) compared to MA ( $\Delta b = 0.19 \pm 0.03$  and  $\Delta w = 0.05 \pm 0.03$ ) at 10 km downwind of the fire source. As the plume is transported to 15 and 20 km downwind, there is significantly more overlap between the GOMECH structure of P(NO<sub>3</sub>) and aerosol NC (71 and, 78% respectively) compared to MA (48 and 56%, respectively). Eventually, the plume center of aerosol NC determined by GOMECH aligns with CO (Table S10), similar to GOMECH results seen in the 7 Aug case for smoke sampled with age > 3 h (Figure S20).

The above conclusions are further supported by correlations of NC aerosol with integrated P(NO<sub>3</sub>) or MA (see Supporting Information and Figure S21), which shows that NC aerosol is best correlated with integrated P(NO<sub>3</sub>) ( $R^2 = 0.72\text{--}0.92$ ) when compared to MA ( $R^2 = 0.35\text{--}0.76$ ) in all four WF plumes we study.

The oxidation of phenolics and formation of nitrophenolics are known to contribute to SOA and BrC formation in BB plumes.<sup>7</sup> Further, NO<sub>3</sub> chemistry has been suggested to

contribute to most of the organic aerosol from wintertime residential wood combustion in at least one analysis.<sup>16</sup> Our analysis suggests that NO<sub>3</sub> chemistry may be a major source of nitrophenolics, even on plume edges, in daytime BB plumes studied during FIREX-AQ, and a dominant (55%) source in our case study.

As shown above and in detail in the Supporting Information, GOMECH is able to resolve spatial heterogeneity in NO<sub>3</sub> and OH chemistry by recreating plume structures within 20% of the observations. Narrower or wider plumes (such as HONO or MA) are better approximated with GOMECH and have lower fit residuals when compared to more complex plume structures with plume center shifts ( $b \neq 0$ , such as MA, PAN, or O<sub>3</sub>). GOMECH is a simple, empirical model that can be fit to aircraft data from discrete emission sources. GOMECH provides a method for studying the spatial heterogeneity of plumes by providing quantitative measures of differential gradients in short-lived species relative to long-lived tracers and, as such, can quantify chemical regimes in chemically evolving plumes. We provide a GOMECH analysis tool for download (see Supporting Information Section 3) to be used by others in future crosswind heterogeneity studies. GOMECH is general and should be independent of factors such as plume injection height, combustion efficiency, turbulence, and so forth. It therefore may find application in urban plumes or plumes from power generation sources. If so, it would provide insights into chemical processes contributing to the evolution of short-lived emissions and their oxidation products.

## ASSOCIATED CONTENT

### Supporting Information

The Supporting Information is available free of charge at <https://pubs.acs.org/doi/10.1021/acs.est.1c03803>.

Aircraft measurement details; LES model details; derivation of GOMECH; introduction to the plume structure model by the example of HONO and  $j_{\text{HONO}}$ ; discussion on uncertainties and model limitations; mechanism of MA formation; supporting figures and tables for bulk analysis; and supporting figures and tables for the WF case study ([PDF](#))

## AUTHOR INFORMATION

### Corresponding Author

**Steven S. Brown** — NOAA Chemical Sciences Laboratory (CSL), Boulder, Colorado 80305, United States; Department of Chemistry, University of Colorado Boulder, Boulder, Colorado 80309-0215, United States;  [orcid.org/0000-0001-7477-9078](https://orcid.org/0000-0001-7477-9078); Email: [steven.s.brown@noaa.gov](mailto:steven.s.brown@noaa.gov)

### Authors

**Zachary C. J. Decker** — NOAA Chemical Sciences Laboratory (CSL), Boulder, Colorado 80305, United States; Cooperative Institute for Research in Environmental Sciences, University of Colorado Boulder, Boulder, Colorado 80309, United States; Department of Chemistry, University of Colorado Boulder, Boulder, Colorado 80309-0215, United States;  [orcid.org/0000-0001-9604-8671](https://orcid.org/0000-0001-9604-8671)

**Siyuan Wang** — NOAA Chemical Sciences Laboratory (CSL), Boulder, Colorado 80305, United States; Cooperative Institute for Research in Environmental Sciences, University of Colorado Boulder, Boulder, Colorado 80309, United States

**Ilann Bourgeois** — NOAA Chemical Sciences Laboratory (CSL), Boulder, Colorado 80305, United States; Cooperative Institute for Research in Environmental Sciences, University of Colorado Boulder, Boulder, Colorado 80309, United States;  [orcid.org/0000-0002-2875-1258](https://orcid.org/0000-0002-2875-1258)

**Pedro Campuzano Jost** — Cooperative Institute for Research in Environmental Sciences, University of Colorado Boulder, Boulder, Colorado 80309, United States; Department of Chemistry, University of Colorado Boulder, Boulder, Colorado 80309-0215, United States;  [orcid.org/0000-0003-3930-010X](https://orcid.org/0000-0003-3930-010X)

**Matthew M. Coggon** — NOAA Chemical Sciences Laboratory (CSL), Boulder, Colorado 80305, United States; Cooperative Institute for Research in Environmental Sciences, University of Colorado Boulder, Boulder, Colorado 80309, United States;  [orcid.org/0000-0002-5763-1925](https://orcid.org/0000-0002-5763-1925)

**Joshua P. DiGangi** — NASA Langley Research Center, Hampton, Virginia 23681, United States

**Glenn S. Diskin** — NASA Langley Research Center, Hampton, Virginia 23681, United States

**Frank M. Flocke** — Atmospheric Chemistry Observations and Modeling Laboratory, National Center for Atmospheric Research, Boulder, Colorado 80301, United States

**Alessandro Franchin** — NOAA Chemical Sciences Laboratory (CSL), Boulder, Colorado 80305, United States; Cooperative Institute for Research in Environmental Sciences, University of Colorado Boulder, Boulder, Colorado 80309, United States; Atmospheric Chemistry Observations and Modeling Laboratory, National Center for Atmospheric Research, Boulder, Colorado 80301, United States

**Carley D. Fredrickson** — Department of Atmospheric Sciences, University of Washington, Seattle, Washington 98195, United States

**Georgios I. Gkatzelis** — NOAA Chemical Sciences Laboratory (CSL), Boulder, Colorado 80305, United States; Cooperative Institute for Research in Environmental Sciences, University of Colorado Boulder, Boulder, Colorado 80309, United States; Present Address: Institute of Energy and Climate Research, IEK-8: Troposphere, Forschungszentrum Jülich GmbH, Jülich, 52428, Germany

**Samuel R. Hall** — Atmospheric Chemistry Observations and Modeling Laboratory, National Center for Atmospheric Research, Boulder, Colorado 80301, United States

**Hannah Halliday** — Atmospheric Chemistry Observations and Modeling Laboratory, National Center for Atmospheric Research, Boulder, Colorado 80301, United States; Present Address: EPA Office of Research and Development, RTP, NC 27711, USA.;  [orcid.org/0000-0001-9499-9836](https://orcid.org/0000-0001-9499-9836)

**Katherine Hayden** — Air Quality Research Division (AQRD), Environment and Climate Change Canada, Toronto M3H 5T4, Canada

**Christopher D. Holmes** — Department of Earth, Ocean, and Atmospheric Science, Florida State University, Tallahassee, Florida 32304, United States;  [orcid.org/0000-0002-2727-0954](https://orcid.org/0000-0002-2727-0954)

**L. Gregory Huey** — School of Earth and Atmospheric Sciences, Georgia Institute of Technology, Atlanta, Georgia 30332, United States;  [orcid.org/0000-0002-0518-7690](https://orcid.org/0000-0002-0518-7690)

**Jose L. Jimenez** — Cooperative Institute for Research in Environmental Sciences, University of Colorado Boulder, Boulder, Colorado 80309, United States; Department of Chemistry, University of Colorado Boulder, Boulder,

- Colorado 80309-0215, United States;  orcid.org/0000-0001-6203-1847
- Young Ro Lee** — School of Earth and Atmospheric Sciences, Georgia Institute of Technology, Atlanta, Georgia 30332, United States
- Jakob Lindaas** — Department of Atmospheric Science, Colorado State University, Fort Collins, Colorado 80523, United States
- Ann M. Middlebrook** — NOAA Chemical Sciences Laboratory (CSL), Boulder, Colorado 80305, United States
- Denise D. Montzka** — Atmospheric Chemistry Observations and Modeling Laboratory, National Center for Atmospheric Research, Boulder, Colorado 80301, United States
- J. Andrew Neuman** — NOAA Chemical Sciences Laboratory (CSL), Boulder, Colorado 80305, United States; Cooperative Institute for Research in Environmental Sciences, University of Colorado Boulder, Boulder, Colorado 80309, United States
- John B. Nowak** — Science Systems and Applications, Inc. (SSAI), Hampton, Virginia 23666, United States;  orcid.org/0000-0002-5697-9807
- Demetrios Pagonis** — Cooperative Institute for Research in Environmental Sciences, University of Colorado Boulder, Boulder, Colorado 80309, United States; Department of Chemistry, University of Colorado Boulder, Boulder, Colorado 80309-0215, United States;  orcid.org/0000-0002-0441-2614
- Brett B. Palm** — Department of Atmospheric Sciences, University of Washington, Seattle, Washington 98195, United States; Present Address: Atmospheric Chemistry Observations and Modeling Laboratory, National Center for Atmospheric Research, Boulder, CO 80301, USA.
- Jeff Peischl** — NOAA Chemical Sciences Laboratory (CSL), Boulder, Colorado 80305, United States; Cooperative Institute for Research in Environmental Sciences, University of Colorado Boulder, Boulder, Colorado 80309, United States
- Felix Piel** — Institute for Ion Physics and Applied Physics, University of Innsbruck, Innsbruck 6020, Austria; Department of Chemistry, University of Oslo, Oslo 0315, Norway
- Pamela S. Rickly** — NOAA Chemical Sciences Laboratory (CSL), Boulder, Colorado 80305, United States; Cooperative Institute for Research in Environmental Sciences, University of Colorado Boulder, Boulder, Colorado 80309, United States
- Michael A. Robinson** — NOAA Chemical Sciences Laboratory (CSL), Boulder, Colorado 80305, United States; Cooperative Institute for Research in Environmental Sciences, University of Colorado Boulder, Boulder, Colorado 80309, United States; Department of Chemistry, University of Colorado Boulder, Boulder, Colorado 80309-0215, United States
- Andrew W. Rollins** — NOAA Chemical Sciences Laboratory (CSL), Boulder, Colorado 80305, United States
- Thomas B. Ryerson** — NOAA Chemical Sciences Laboratory (CSL), Boulder, Colorado 80305, United States; Present Address: Scientific Aviation, Inc., 3335 Airport Road Suite B, Boulder, Colorado 80301, United States.
- Kanako Sekimoto** — Graduate School of Nanobioscience, Yokohama City University, Yokohama 236-0027, Japan;  orcid.org/0000-0001-9908-9698
- Joel A. Thornton** — Department of Atmospheric Sciences, University of Washington, Seattle, Washington 98195, United States;  orcid.org/0000-0002-5098-4867
- Geoff S. Tyndall** — Atmospheric Chemistry Observations and Modeling Laboratory, National Center for Atmospheric Research, Boulder, Colorado 80301, United States
- Kirk Ullmann** — Atmospheric Chemistry Observations and Modeling Laboratory, National Center for Atmospheric Research, Boulder, Colorado 80301, United States
- Patrick R. Veres** — NOAA Chemical Sciences Laboratory (CSL), Boulder, Colorado 80305, United States
- Carsten Warneke** — NOAA Chemical Sciences Laboratory (CSL), Boulder, Colorado 80305, United States; Cooperative Institute for Research in Environmental Sciences, University of Colorado Boulder, Boulder, Colorado 80309, United States;  orcid.org/0000-0003-3811-8496
- Rebecca A. Washenfelder** — NOAA Chemical Sciences Laboratory (CSL), Boulder, Colorado 80305, United States
- Andrew J. Weinheimer** — Atmospheric Chemistry Observations and Modeling Laboratory, National Center for Atmospheric Research, Boulder, Colorado 80301, United States
- Armin Wisthaler** — Institute for Ion Physics and Applied Physics, University of Innsbruck, Innsbruck 6020, Austria; Department of Chemistry, University of Oslo, Oslo 0315, Norway;  orcid.org/0000-0001-5050-3018
- Caroline Womack** — NOAA Chemical Sciences Laboratory (CSL), Boulder, Colorado 80305, United States; Cooperative Institute for Research in Environmental Sciences, University of Colorado Boulder, Boulder, Colorado 80309, United States

Complete contact information is available at:  
<https://pubs.acs.org/10.1021/acs.est.1c03803>

## Notes

The authors declare no competing financial interest.

## ACKNOWLEDGMENTS

We thank Reed Meyerson for his assistance in deriving <sup>eq 2</sup>, and Charlie Edelson for his thoughtful conversation on the intricacies of multivariable regression. The UIBK PTR-ToF-MS instrument was partly funded by the Austrian Federal Ministry for Transport, Innovation and Technology (bmvit) through the Austrian Space Applications Programme (ASAP) of the Austrian Research Promotion Agency (FFG). Instrumental support came from Ionicon Analytik; Tomas Mikoviny provided technical assistance. Laura Tomsche and John Nowak supported the UIBK PTR-ToF-MS team. F.P. received funding from the European Union's Horizon 2020 research and innovation program under grant agreement no. 674911 (IMPACT EU ITN). The Jimenez group (CU Boulder) acknowledges funding from NASA grant 80NSSC18K0630. The Thornton group (Univ. Washington) was supported by grants from the National Oceanic and Atmospheric Administration (NA17OAR4310012) and the National Science Foundation (AGS 1652688).

## REFERENCES

- (1) Jaffe, D. A.; O'Neill, S. M.; Larkin, N. K.; Holder, A. L.; Peterson, D. L.; Halofsky, J. E.; Rappold, A. G. Wildfire and Prescribed Burning Impacts on Air Quality in the United States. *J. Air Waste Manag. Assoc.* **2020**, *70*, 583–615.
- (2) Akagi, S. K.; Yokelson, R. J.; Wiedinmyer, C.; Alvarado, M. J.; Reid, J. S.; Karl, T.; Crounse, J. D.; Wennberg, P. O. Emission Factors for Open and Domestic Biomass Burning for Use in Atmospheric Models. *Atmos. Chem. Phys.* **2011**, *11*, 4039–4072.

- (3) Hatch, L. E.; Luo, W.; Pankow, J. F.; Yokelson, R. J.; Stockwell, C. E.; Barsanti, K. C. Identification and Quantification of Gaseous Organic Compounds Emitted from Biomass Burning Using Two-Dimensional Gas Chromatography–Time-of-Flight Mass Spectrometry. *Atmos. Chem. Phys.* **2015**, *15*, 1865–1899.
- (4) Hatch, L. E.; Yokelson, R. J.; Stockwell, C. E.; Veres, P. R.; Simpson, I. J.; Blake, D. R.; Orlando, J. J.; Barsanti, K. C. Multi-Instrument Comparison and Compilation of Non-Methane Organic Gas Emissions from Biomass Burning and Implications for Smoke-Derived Secondary Organic Aerosol Precursors. *Atmos. Chem. Phys.* **2017**, *17*, 1471–1489.
- (5) Koss, A. R.; Sekimoto, K.; Gilman, J. B.; Selimovic, V.; Coggon, M. M.; Zarzana, K. J.; Yuan, B.; Lerner, B. M.; Brown, S. S.; Jimenez, J. L.; Krechmer, J.; Roberts, J. M.; Warneke, C.; Yokelson, R. J.; de Gouw, J. Non-Methane Organic Gas Emissions from Biomass Burning: Identification, Quantification, and Emission Factors from PTR-ToF during the FIREX 2016 Laboratory Experiment. *Atmos. Chem. Phys.* **2018**, *18*, 3299–3319.
- (6) Andreae, M. O.; Merlet, P. Emissions of Trace Gases and Aerosols from Biomass Burning. *Biogeochemistry* **2001**, *15*, 955–966.
- (7) Palm, B. B.; Peng, Q.; Fredrickson, C. D.; Lee, B. H.; Garofalo, L. A.; Pothier, M. A.; Kreidenweis, S. M.; Farmer, D. K.; Pokhrel, R. P.; Shen, Y.; Murphy, S. M.; Permar, W.; Hu, L.; Campos, T. L.; Hall, S. R.; Ullmann, K.; Zhang, X.; Flocke, F.; Fischer, E. V.; Thornton, J. A. Quantification of Organic Aerosol and Brown Carbon Evolution in Fresh Wildfire Plumes. *Proc. Natl. Acad. Sci. U.S.A.* **2020**, *117*, 29469–29477.
- (8) Decker, Z. C. J.; Zarzana, K. J.; Coggon, M.; Min, K.-E.; Pollack, I.; Ryerson, T. B.; Peischl, J.; Edwards, P.; Dubé, W. P.; Markovic, M. Z.; Roberts, J. M.; Veres, P. R.; Graus, M.; Warneke, C.; de Gouw, J.; Hatch, L. E.; Barsanti, K. C.; Brown, S. S. Nighttime Chemical Transformation in Biomass Burning Plumes: A Box Model Analysis Initialized with Aircraft Observations. *Environ. Sci. Technol.* **2019**, *53*, 2529–2538.
- (9) Brown, S. S.; Dubé, W. P.; Karamchandani, P.; Yarwood, G.; Peischl, J.; Ryerson, T. B.; Neuman, J. A.; Nowak, J. B.; Holloway, J. S.; Washenfelder, R. A.; Brock, C. A.; Frost, G. J.; Trainer, M.; Parrish, D. D.; Fehsenfeld, F. C.; Ravishankara, A. R. Effects of NO<sub>x</sub> Control and Plume Mixing on Nighttime Chemical Processing of Plumes from Coal-Fired Power Plants. *J. Geophys. Res. Atmos.* **2012**, *117*, D07304.
- (10) Jones, R. L.; Ball, S. M.; Shallcross, D. E. Small Scale Structure in the Atmosphere: Implications for Chemical Composition and Observational Methods. *Faraday Discuss.* **2005**, *130*, 165–179.
- (11) Meidan, D.; Holloway, J. S.; Edwards, P. M.; Dubé, W. P.; Middlebrook, A. M.; Liao, J.; Welti, A.; Graus, M.; Warneke, C.; Ryerson, T. B.; Pollack, I. B.; Brown, S. S.; Rudich, Y. Role of Criegee Intermediates in Secondary Sulfate Aerosol Formation in Nocturnal Power Plant Plumes in the Southeast US. *ACS Earth Space Chem.* **2019**, *3*, 748–759.
- (12) Peng, Q.; Palm, B. B.; Melander, K. E.; Lee, B. H.; Hall, S. R.; Ullmann, K.; Campos, T.; Weinheimer, A. J.; Apel, E. C.; Hornbrook, R. S.; Hills, A. J.; Montzka, D. D.; Flocke, F.; Hu, L.; Permar, W.; Wielgasz, C.; Lindaas, J.; Pollack, I. B.; Fischer, E. V.; Bertram, T. H.; Thornton, J. A. HONO Emissions from Western U.S. Wildfires Provide Dominant Radical Source in Fresh Wildfire Smoke. *Environ. Sci. Technol.* **2020**, *54*, 5954–5963.
- (13) Decker, Z. C. J.; Robinson, M. A.; Barsanti, K. C.; Bourgeois, I.; Matthew, M.; Digangi, J. P.; Diskin, G. S.; Flocke, F. M.; Franchin, A.; Carley, D.; Hall, S. R.; Halliday, H.; Holmes, C. D.; Huey, L. G.; Lee, R.; Lindaas, J.; Middlebrook, A. M.; Montzka, D. D.; Moore, R.; Andrew, J.; Nowak, J. B.; Palm, B. B.; Peischl, J.; Rickly, P. S.; Rollins, A. W.; Ryerson, T. B.; Schwantes, R. H.; Thornhill, L.; Thornton, J. A.; Geoffrey, S.; Ullmann, K.; Rooy, P. V.; Veres, P. R.; Weinheimer, A. J.; Winstead, E.; Womack, C.; Brown, S. S. Nighttime and Daytime Dark Oxidation Chemistry in Wildfire Plumes: An Observation and Model Analysis of FIREX-AQ Aircraft Data. *Atmos. Chem. Phys. Discuss.* **2021**, *21*, 16293.
- (14) Gouw, J. A.; Parrish, D. D.; Brown, S. S.; Edwards, P.; Gilman, J. B.; Graus, M.; Hanisco, T. F.; Kaiser, J.; Keutsch, F. N.; Kim, S. W.; Lerner, B. M.; Neuman, J. A.; Nowak, J. B.; Pollack, I. B.; Roberts, J. M.; Ryerson, T. B.; Veres, P. R.; Warneke, C.; Wolfe, G. M. Hydrocarbon Removal in Power Plant Plumes Shows Nitrogen Oxide Dependence of Hydroxyl Radicals. *Geophys. Res. Lett.* **2019**, *46*, 7752–7760.
- (15) Trentmann, J.; Andreae, M. O.; Graf, H. F. Chemical Processes in a Young Biomass-Burning Plume. *J. Geophys. Res. Atmos.* **2003**, *108*, 4705.
- (16) Kodros, J. K.; Papanastasiou, D. K.; Paglione, M.; Masiol, M.; Squizzato, S.; Florou, K.; Skyllakou, K.; Kaltsonoudis, C.; Nenes, A.; Pandis, S. N. The Oxidizing Power of the Dark Side: Rapid Nocturnal Aging of Biomass Burning as an Overlooked Source of Oxidized Organic Aerosol. *Proc. Natl. Acad. Sci. U.S.A.* **2020**, *117*, 33028–33033.
- (17) Keywood, M.; Cope, M.; Meyer, C. P. M.; Iinuma, Y.; Emmerson, K. When Smoke Comes to Town: The Impact of Biomass Burning Smoke on Air Quality. *Atmos. Environ.* **2015**, *121*, 13–21.
- (18) Wayne, R. P.; Barnes, I.; Biggs, P.; Burrows, J. P.; Canosa-Mas, C. E.; Hjorth, J.; Le Bras, G.; Moortgat, G. K.; Perner, D.; Poulet, G.; Restelli, G.; Sidebottom, H. The Nitrate Radical: Physics, Chemistry, and the Atmosphere. *Atmos. Environ., Part A* **1991**, *25*, 1–203.
- (19) Brown, S. S.; Stutz, J. Nighttime Radical Observations and Chemistry. *Chem. Soc. Rev.* **2012**, *41*, 6405–6447.
- (20) Chang, W. L.; Bhave, P. V.; Brown, S. S.; Riemer, N.; Stutz, J.; Dabdub, D. Heterogeneous Atmospheric Chemistry, Ambient Measurements, and Model Calculations of N<sub>2</sub>O<sub>5</sub>: A Review. *Aerosol Sci. Technol.* **2011**, *45*, 655–685.
- (21) McDuffie, E. E.; Fibiger, D. L.; Dubé, W. P.; Lopez-Hilfiker, F.; Lee, B. H.; Thornton, J. A.; Shah, V.; Jaeglé, L.; Guo, H.; Weber, R. J.; Michael Reeves, J.; Weinheimer, A. J.; Schroder, J. C.; Campuzano-Jost, P.; Jimenez, J. L.; Dibb, J. E.; Veres, P.; Ebbesen, C.; Sparks, T. L.; Wooldridge, P. J.; Cohen, R. C.; Hornbrook, R. S.; Apel, E. C.; Campos, T.; Hall, S. R.; Ullmann, K.; Brown, S. S. Heterogeneous N<sub>2</sub>O<sub>5</sub> Uptake During Winter: Aircraft Measurements During the 2015 WINTER Campaign and Critical Evaluation of Current Parameterizations. *J. Geophys. Res. Atmos.* **2018**, *123*, 4345–4372.
- (22) Finewax, Z.; De Gouw, J. A.; Ziemann, P. J. Identification and Quantification of 4-Nitrocatechol Formed from OH and NO<sub>3</sub> Radical-Initiated Reactions of Catechol in Air in the Presence of NO<sub>x</sub>: Implications for Secondary Organic Aerosol Formation from Biomass Burning. *Environ. Sci. Technol.* **2018**, *52*, 1981–1989.
- (23) Xie, M.; Chen, X.; Hays, M. D.; Lewandowski, M.; Offenberg, J.; Kleindienst, T. E.; Holder, A. L. Light Absorption of Secondary Organic Aerosol: Composition and Contribution of Nitroaromatic Compounds. *Environ. Sci. Technol.* **2017**, *51*, 11607–11616.
- (24) Liu, C.; Liu, J.; Liu, Y.; Chen, T.; He, H. Secondary Organic Aerosol Formation from the OH-Initiated Oxidation of Guaiacol under Different Experimental Conditions. *Atmos. Environ.* **2019**, *207*, 30–37.
- (25) Lauraguais, A.; Coeur-Tourneur, C.; Cassez, A.; Deboudt, K.; Fourmentin, M.; Choël, M. Atmospheric Reactivity of Hydroxyl Radicals with Guaiacol (2-Methoxyphenol), a Biomass Burning Emitted Compound: Secondary Organic Aerosol Formation and Gas-Phase Oxidation Products. *Atmos. Environ.* **2014**, *86*, 155–163.
- (26) Selimovic, V.; Yokelson, R. J.; McMeeking, G. R.; Coefield, S. Aerosol Mass and Optical Properties, Smoke Influence on O<sub>3</sub>, and High NO<sub>3</sub> Production Rates in a Western U.S. City Impacted by Wildfires. *J. Geophys. Res. Atmos.* **2020**, *125*, No. e2020JD032791.
- (27) White, W. H.; Anderson, J. A.; Blumenthal, D. L.; Husar, R. B.; Gillani, N. V.; Husar, J. D.; Wilson, W. E. Formation and Transport of Secondary Air Pollutants: Ozone and Aerosols in the St. Louis Urban Plume. *Science* **1976**, *194*, 187–189.
- (28) Jost, C.; Trentmann, J.; Sprung, D.; Andreae, M. O.; Quaid, J. B.; Barjat, H. Trace Gas Chemistry in a Young Biomass Burning Plume over Namibia: Observations and Model Simulations. *J. Geophys. Res. Atmos.* **2003**, *108*, 8482.
- (29) Brock, C. A.; Trainer, M.; Ryerson, T. B.; Neuman, J. A.; Parrish, D. D.; Holloway, J. S.; Nicks, D. K.; Frost, G. J.; Hübner, G.; Fehsenfeld, F. C.; Wilson, J. C.; Reeves, J. M.; Lafleur, B. G.; Hilbert,

- H.; Atlas, E. L.; Donnelly, S. G.; Schauffler, S. M.; Stroud, V. R.; Wiedinmyer, C. Particle Growth in Urban and Industrial Plumes in Texas. *J. Geophys. Res. Atmos.* **2003**, *108*, 4111.
- (30) Trentmann, J.; Yokelson, R. J.; Hobbs, P. V.; Winterrath, T.; Christian, T. J.; Andreae, M. O.; Mason, S. A. An Analysis of the Chemical Processes in the Smoke Plume from a Savanna Fire. *J. Geophys. Res. Atmos.* **2005**, *110*, D12301.
- (31) Müller, M.; Anderson, B. E.; Beyersdorf, A. J.; Crawford, J. H.; Diskin, G. S.; Eichler, P.; Fried, A.; Keutsch, F. N.; Mikoviny, T.; Thornhill, K. L.; Walega, J. G.; Weinheimer, A. J.; Yang, M.; Yokelson, R. J.; Wisthaler, A. In Situ Measurements and Modeling of Reactive Trace Gases in a Small Biomass Burning Plume. *Atmos. Chem. Phys.* **2016**, *16*, 3813–3824.
- (32) Neuman, J. A.; Trainer, M.; Brown, S. S.; Min, K.-E.; Nowak, J. B.; Parrish, D. D.; Peischl, J.; Pollack, I. B.; Roberts, J. M.; Ryerson, T. B.; Veres, P. R. HONO Emission and Production Determined from Airborne Measurements over the Southeast U.S. *J. Geophys. Res.* **2016**, *121*, 9237–9250.
- (33) Wang, Y.; Hu, M.; Lin, P.; Guo, Q.; Wu, Z.; Li, M.; Zeng, L.; Song, Y.; Zeng, L.; Wu, Y.; Guo, S.; Huang, X.; He, L. Molecular Characterization of Nitrogen-Containing Organic Compounds in Humic-like Substances Emitted from Straw Residue Burning. *Environ. Sci. Technol.* **2017**, *51*, 5951–5961.
- (34) Trentmann, J.; Andreae, M. O.; Graf, H. F.; Hobbs, P. V.; Ottmar, R. D.; Trautmann, T. Simulation of a Biomass-Burning Plume: Comparison of Model Results with Observations. *J. Geophys. Res. Atmos.* **2002**, *107*, 4013.
- (35) Alvarado, M. J.; Prinn, R. G. Formation of Ozone and Growth of Aerosols in Young Smoke Plumes from Biomass Burning: 1. Lagrangian Parcel Studies. *J. Geophys. Res. Atmos.* **2009**, *114*, D09306.
- (36) Wang, S.; Coggon, M. M.; Gkatzelis, G. I.; Warneke, C.; Bourgeois, I.; Ryerson, T.; Peischl, J.; Veres, P. R.; Neuman, J. A.; Hair, J.; Shingler, T.; Fenn, M.; Diskin, G.; Huey, L. G.; Lee, Y. R.; Apel, E. C.; Hornbrook, R. S.; Hills, A. J.; Hall, S. R.; Ullmann, K.; Bela, M. M.; Trainer, M. K.; Kumar, R.; Orlando, J. J.; Flocke, F. M.; Emmons, L. K. Chemical Tomography in a Fresh Wildland Fire Plume: A Large Eddy Simulation (LES) Study. *J. Geophys. Res. Atmos.* **2021**, *126*, No. e2021JD035203.
- (37) Holmes, C. D.; Fite, C. H.; Agastra, A.; SchwarzJoshua, P.; Yokelson, R. J.; Bui, T. P.; Kondragunta, S.; Peterson, D. A. Critical Evaluation of Smoke Age Inferred from Different Methods during FIREX-AQ. AGU Fall Meeting 2020, 2020.
- (38) Lee, B. H.; Lopez-Hilfiker, F. D.; Mohr, C.; Kurtén, T.; Worsnop, D. R.; Thornton, J. A. An Iodide-Adduct High-Resolution Time-of-Flight Chemical-Ionization Mass Spectrometer: Application to Atmospheric Inorganic and Organic Compounds. *Environ. Sci. Technol.* **2014**, *48*, 6309–6317.
- (39) Crosson, E. R. A Cavity Ring-down Analyzer for Measuring Atmospheric Levels of Methane, Carbon Dioxide, and Water Vapor. *Appl. Phys. B: Lasers Opt.* **2008**, *92*, 403–408.
- (40) Sparks, T. L.; Ebbin, C. J.; Wooldridge, P. J.; Lopez-Hilfiker, F. D.; Lee, B. H.; Thornton, J. A.; McDuffie, E. E.; Fibiger, D. L.; Brown, S. S.; Montzka, D. D.; Weinheimer, A. J.; Schroder, J. C.; Campuzano-Jost, P.; Jimenez, J. L.; Cohen, R. C. Comparison of Airborne Reactive Nitrogen Measurements During WINTER. *J. Geophys. Res. Atmos.* **2019**, *124*, 10483–10502.
- (41) Liggio, J.; Li, S.-M.; Hayden, K.; Taha, Y. M.; Stroud, C.; Darlington, A.; Drollette, B. D.; Gordon, M.; Lee, P.; Liu, P.; Leithead, A.; Moussa, S. G.; Wang, D.; O'Brien, J.; Mittermeier, R. L.; Brook, J. R.; Lu, G.; Staebler, R. M.; Han, Y.; Tokarek, T. W.; Osthoff, H. D.; Makar, P. A.; Zhang, J.; Plata, D. L.; Gentner, D. R. Oil Sands Operations as a Large Source of Secondary Organic Aerosols. *Nature* **2016**, *534*, 91–94.
- (42) Decarlo, P. F.; Kimmel, J. R.; Trimborn, A.; Northway, M. J.; Jayne, J. T.; Aiken, A. C.; Gonin, M.; Fuhrer, K.; Horvath, T.; Docherty, K. S.; Worsnop, D. R.; Jimenez, J. L. Field-Deployable, High-Resolution, Time-of-Flight Aerosol Mass Spectrometer. *Anal. Chem.* **2006**, *78*, 8281–8289.
- (43) Sachse, G. W.; Collins, J. E., Jr.; Hill, G. F.; Wade, L. O.; Lewis, B. G.; Ritter, J. A. Airborne Tunable Diode Laser Sensor for High-Precision Concentration and Flux Measurements of Carbon Monoxide and Methane. *Proc. SPIE* **1991**, *1433*, 157–166.
- (44) Eilerman, S. J.; Peischl, J.; Neuman, J. A.; Ryerson, T. B.; Aikin, K. C.; Holloway, M. W.; Zondlo, M. A.; Golston, L. M.; Pan, D.; Floerchinger, C.; Herndon, S. Characterization of Ammonia, Methane, and Nitrous Oxide Emissions from Concentrated Animal Feeding Operations in Northeastern Colorado. *Environ. Sci. Technol.* **2016**, *50*, 10885–10893.
- (45) Pollack, I. B.; Lerner, B. M.; Ryerson, T. B. Evaluation of Ultraviolet Light-Emitting Diodes for Detection of Atmospheric NO<sub>2</sub> by Photolysis - Chemiluminescence. *J. Atmos. Chem.* **2010**, *65*, 111–125.
- (46) Ridley, B. A.; Grahek, F. E.; Walega, J. G. A Small High-Sensitivity, Medium-Response Ozone Detector Suitable for Measurements from Light Aircraft. *J. Atmos. Ocean. Technol.* **1992**, *9*, 142–148.
- (47) Stedman, D. H.; Daby, E. E.; Stuhl, F.; Niki, H. Analysis of Ozone and Nitric Oxide by a Chemiluminescent Method in Laboratory and Atmospheric Studies of Photochemical Smog. *J. Air Pollut. Control Assoc.* **1972**, *22*, 260–263.
- (48) Min, K.-E.; Washenfelder, R. a.; Dubé, W. P.; Langford, a. O.; Edwards, P. M.; Zarzana, K. J.; Stutz, J.; Lu, K.; Rohrer, F.; Zhang, Y.; Brown, S. S. A Broadband Cavity Enhanced Absorption Spectrometer for Aircraft Measurements of Glyoxal, Methylglyoxal, Nitrous Acid, Nitrogen Dioxide, and Water Vapor. *Atmos. Meas. Tech. Discuss.* **2016**, *9*, 423–440.
- (49) Rollins, A. W.; Rickly, P. S.; Gao, R.-S.; Ryerson, T. B.; Brown, S. S.; Peischl, J.; Bourgeois, I. Single-Photon Laser-Induced Fluorescence Detection of Nitric Oxide at Sub-Parts-per-Trillion Mixing Ratios. *Atmos. Meas. Tech.* **2020**, *13*, 2425–2439.
- (50) Coggon, M. M.; Lim, C. Y.; Koss, A. R.; Sekimoto, K.; Yuan, B.; Gilman, J. B.; Hagan, D. H.; Selimovic, V.; Zarzana, K. J.; Brown, S. S.; Roberts, J. M.; Müller, M.; Yokelson, R.; Wisthaler, A.; Krechmer, J. E.; Jimenez, J. L.; Cappa, C.; Kroll, J. H.; De Gouw, J.; Warneke, C. OH Chemistry of Non-Methane Organic Gases (NMOGs) Emitted from Laboratory and Ambient Biomass Burning Smoke: Evaluating the Influence of Furans and Oxygenated Aromatics on Ozone and Secondary NMOG Formation. *Atmos. Chem. Phys.* **2019**, *19*, 14875–14899.
- (51) Müller, M.; Mikoviny, T.; Feil, S.; Haidacher, S.; Hanel, G.; Hartungen, E.; Jordan, A.; Märk, L.; Mutschlechner, P.; Schottkowsky, R.; Sulzer, P.; Crawford, J. H.; Wisthaler, A. A Compact PTR-ToF-MS Instrument for Airborne Measurements of Volatile Organic Compounds at High Spatiotemporal Resolution. *Atmos. Meas. Tech.* **2014**, *7*, 3763–3772.
- (52) Piel, F.; Müller, M.; Winkler, K.; Skytte af Sätra, J.; Wisthaler, A. Introducing the Extended Volatility Range Proton-Transfer-Reaction Mass Spectrometer (EVR PTR-MS). *Atmos. Meas. Tech.* **2021**, *14*, 1355–1363.
- (53) Piel, F.; Müller, M.; Mikoviny, T.; Pusede, S. E.; Wisthaler, A. Airborne Measurements of Particulate Organic Matter by Proton-Transfer-Reaction Mass Spectrometry (PTR-MS): A Pilot Study. *Atmos. Meas. Tech.* **2019**, *12*, 5947–5958.
- (54) Veres, P. R.; Neuman, J. A.; Bertram, T. H.; Assaf, E.; Wolfe, G. M.; Williamson, C. J.; Weinzierl, B.; Tilmes, S.; Thompson, C. R.; Thames, A. B.; Schroder, J. C.; Saiz-Lopez, A.; Rollins, A. W.; Roberts, J. M.; Price, D.; Peischl, J.; Nault, B. A.; Möller, K. H.; Miller, D. O.; Meinardi, S.; Li, Q.; Lamarque, J.-F.; Kupc, A.; Kjaergaard, H. G.; Kinnison, D.; Jimenez, J. L.; Jernigan, C. M.; Hornbrook, R. S.; Hills, A.; Dollner, M.; Day, D. A.; Cuevas, C. A.; Campuzano-Jost, P.; Burkholder, J.; Bui, T. P.; Brune, W. H.; Brown, S. S.; Brock, C. A.; Bourgeois, I.; Blake, D. R.; Apel, E. C.; Ryerson, T. B. Global Airborne Sampling Reveals a Previously Unobserved Dimethyl Sulfide Oxidation Mechanism in the Marine Atmosphere. *Proc. Natl. Acad. Sci. U.S.A.* **2020**, *117*, 4505–4510.
- (55) Lee, Y. R.; Ji, Y.; Tanner, D. J.; Huey, L. G. A Low-Activity Ion Source for Measurement of Atmospheric Gases by Chemical

- Ionization Mass Spectrometry. *Atmos. Meas. Tech.* **2020**, *13*, 2473–2480.
- (56) Pagonis, D.; Campuzano-Jost, P.; Guo, H.; Day, D.; Schueneman, M.; Brown, W.; Nault, B.; Stark, H.; Siemens, K.; Laskin, A.; Piel, F.; Tomsche, L.; Wisthaler, A.; Coggon, M.; Gkatzelis, G.; Halliday, H.; Krechmer, J.; Moore, R.; Thomson, D.; Warneke, C.; Wiggins, E.; Jimenez, J. Airborne Extractive Electrospray Mass Spectrometry Measurements of the Chemical Composition of Organic Aerosol. *Atmos. Meas. Tech. Discuss.* **2021**, *14*, 1545.
- (57) Guo, H.; Campuzano-Jost, P.; Nault, B.; Day, D.; Schroder, J.; Dibb, J.; Dollner, M.; Weinzierl, B.; Jimenez, J. The Importance of Size Ranges in Aerosol Instrument Intercomparisons: A Case Study for the ATom Mission. *Atmos. Meas. Tech.* **2021**, *14*, 3631.
- (58) Nault, B. A.; Campuzano-Jost, P.; Day, D. A.; Schroder, J. C.; Anderson, B.; Beyersdorf, A. J.; Blake, D. R.; Brune, W. H.; Choi, Y.; Corr, C. A.; De Gouw, J. A.; Dibb, J.; Digangi, J. P.; Diskin, G. S.; Fried, A.; Huey, L. G.; Kim, M. J.; Knote, C. J.; Lamb, K. D.; Lee, T.; Park, T.; Pusede, S. E.; Scheuer, E.; Thornhill, K. L.; Woo, J.-H.; Jimenez, J. L. Secondary Organic Aerosol Production from Local Emissions Dominates the Organic Aerosol Budget over Seoul, South Korea, during KORUS-AQ. *Atmos. Chem. Phys.* **2018**, *18*, 17769–17800.
- (59) Shetter, R. E.; Müller, M. Photolysis Frequency Measurements Using Actinic Flux Spectroradiometry during the PEM-Tropics Mission: Instrumentation Description and Some Results. *J. Geophys. Res. Atmos.* **1999**, *104*, 5647–5661.
- (60) Li, F.; Zhang, X.; Kondragunta, S.; Schmidt, C. C.; Holmes, C. D. A Preliminary Evaluation of GOES-16 Active Fire Product Using Landsat-8 and VIIRS Active Fire Data, and Ground-Based Prescribed Fire Records. *Remote Sens. Environ.* **2020**, *237*, 111600.
- (61) Tie, X.; Madronich, S.; Walters, S.; Zhang, R.; Rasch, P.; Collins, W. Effect of Clouds on Photolysis and Oxidants in the Troposphere. *J. Geophys. Res.* **2003**, *108*, 4642.
- (62) Turner, D. B. *Workbook of Atmospheric Dispersion Estimates: An Introduction to Dispersion Modeling*, 2nd ed.; Public Health Services: Cincinnati, 1970.
- (63) Yuan, Y.; Zhao, X.; Wang, S.; Wang, L. Atmospheric Oxidation of Furan and Methyl-Substituted Furans Initiated by Hydroxyl Radicals. *J. Phys. Chem. A* **2017**, *121*, 9306–9319.
- (64) Aschmann, S. M.; Nishino, N.; Arey, J.; Atkinson, R. Products of the OH Radical-Initiated Reactions of Furan, 2- and 3-Methylfuran, and 2,3- and 2,5-Dimethylfuran in the Presence of NO. *J. Phys. Chem. A* **2014**, *118*, 457–466.
- (65) Aschmann, S. M.; Nishino, N.; Arey, J.; Atkinson, R. Kinetics of the Reactions of OH Radicals with 2-and 3-Methylfuran, 2,3-and 2,5-Dimethylfuran, and e -and Z -3-Hexene-2,5-Dione, and Products of OH + 2,5-Dimethylfuran. *Environ. Sci. Technol.* **2011**, *45*, 1859–1865.
- (66) Tapia, A.; Villanueva, F.; Salgado, M. S.; Cabañas, B.; Martínez, E.; Martín, P. Atmospheric Degradation of 3-Methylfuran: Kinetic and Products Study. *Atmos. Chem. Phys.* **2011**, *11*, 3227–3241.
- (67) Bierbach, A.; Barnes, I.; Becker, K. H.; Wiesen, E. Atmospheric Chemistry of Unsaturated Carbonyls: Butenedial, 4-Oxo-2-Pentenal, 3-Hexene-2,5-Dione, Maleic Anhydride, 3H-Furan-2-One, and 5-Methyl-3H-Furan-2-One. *Environ. Sci. Technol.* **1994**, *28*, 715–729.
- (68) Chattopadhyay, A.; Papadimitriou, V. C.; Marshall, P.; Burkholder, J. B. Temperature-Dependent Rate Coefficients for the Gas-Phase OH + Furan-2 , 5-Dione ( C 4 H 2 O 3 , Maleic Anhydride ) Reaction. *Int. J. Chem. Kinet.* **2020**, *52*, 623–631.
- (69) Mellouki, A.; Ammann, M.; Cox, R. A.; Crowley, J. N.; Herrmann, H.; Jenkin, M. E.; McNeill, V. F.; Troe, J.; Wallington, T. J. Evaluated Kinetic and Photochemical Photochemical Data for Atmospheric Chemistry: Volume VIII - Gas-Phase Reactions of Organic Species with Four, or More, Carbon Atoms (= C4). *Atmos. Chem. Phys.* **2021**, *21*, 4797–4808.
- (70) Sangwan, M.; Zhu, L. Absorption Cross Sections of 2-Nitrophenol in the 295–400 nm Region and Photolysis of 2-Nitrophenol at 308 and 351 nm. *J. Phys. Chem. A* **2016**, *120*, 9958–9967.
- (71) Sangwan, M.; Zhu, L. Role of Methyl-2-Nitrophenol Photolysis as a Potential Source of OH Radicals in the Polluted Atmosphere: Implications from Laboratory Investigation. *J. Phys. Chem. A* **2018**, *122*, 1861–1872.